Inorganic Chemistry

Article

pubs.acs.org/IC

Electrochemistry, Chemical Reactivity, and Time-Resolved Infrared Spectroscopy of Donor–Acceptor Systems [(Q^x)Pt(pap^y)] (Q = Substituted *o*-Quinone or *o*-Iminoquinone; pap = Phenylazopyridine)

Naina Deibel,[†] David Schweinfurth,[‡] Stephan Hohloch,[‡] Milan Delor,[∥] Igor V. Sazanovich,[∥] Michael Towrie,[§] Julia A. Weinstein,*[,∥] and Biprajit Sarkar*[,‡]

[†]Institut für Anorganische Chemie, Universität Stuttgart, Pfaffenwaldring 55, D-70569 Stuttgart, Germany

[‡]Institut für Chemie und Biochemie, Freie Universität Berlin, Fabeckstraße 34–36, D-14195 Berlin, Germany

[§]Central Laser Facility, Research Complex at Harwell, Rutherford Appleton Laboratory, Harwell Science and Innovation Campus, STFC, Chilton, Oxfordshire OX11 0QX, U.K.

[∥]Department of Chemistry, University of Sheffield, Sheffield S3 7HF, U.K.

Supporting Information

ABSTRACT: The donor–acceptor complex [($^{O,N}Q^{2-}$)Pt(pap^0)] (**1**; pap = phenylazopyridine, $^{O,N}Q^0$ = 4,6-di-*tert*-butyl-*N*-phenyl-*o*-iminobenzoquinone), which displays strong π-bonding interactions and shows strong absorption in the near-IR region, has been investigated with respect to its redox-induced reactivity and electrochemical and excited-state properties. The one-electron-oxidized product [($^{O,N}Q^{\bullet-}$)Pt(pap^0)](BF_4) ([**1**]BF_4) was chemically isolated. Single-crystal X-ray diffraction studies establish the iminosemiquinone form of $^{O,N}Q$ in $[\mathbf{1}]^+$. Simulation of the cyclic voltammograms of **1** recorded in the presence of PPh_3 elucidates the mechanism and delivers relevant thermodynamic and kinetic parameters for the redox-induced reaction with PPh_3. The thermodynamically stable product of this reaction, complex [($^{O,N}Q^{\bullet-}$)Pt(PPh_3)$_2$](PF_6) ([**2**]PF_6), was isolated and characterized by X-ray crystallography, electrochemistry, and electron paramagnetic resonance spectroscopy. Picosecond time-resolved infrared spectroscopic studies on complex **1b** (one of the positional isomers of **1**) and its analogue [($^{O,O}Q^{2-}$)Pt(pap^0)] (**3**; $^{O,O}Q$ = 3,5-di-*tert*-butyl-*o*-benzoquinone) provided insight into the excited-state dynamics and revealed that the nature of the lowest excited state in the amidophenolate complex **1b** is primarily diimine-ligand-based, while it is predominantly an interligand charge-transfer state in the case of **3**. Density functional theory calculations on $[\mathbf{1}]^{n+}$ provided further insight into the nature of the frontier orbitals of various redox forms and vibrational mode assignments. We discuss the mechanistic details of the newly established redox-induced reactivity of **1** with electron donors and propose a mechanism for this process.

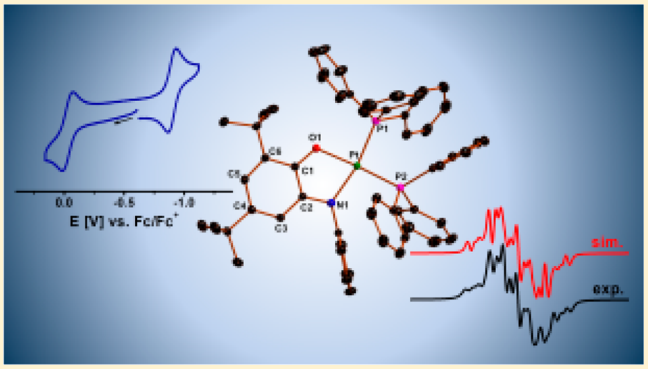

INTRODUCTION

Donor–acceptor systems based on platinum(II) and two different noninnocent ligands have been investigated intensively because of their potential role in harnessing solar energy and their rich redox properties.[1,2] Metal complexes of noninnocent ligands, once considered spectroscopic curiosities,[3] have made a huge comeback in recent years mainly owing to their use in catalysis and energy-related research.[4] Some of us have been involved in the investigation of donor–acceptor complexes of the form [(Q^{2-})Pt(pap^0)] (pap = phenylazopyridine;[5] Q = $^{O,N}Q^0$ = 4,6-di-*tert*-butyl-*N*-phenyl-*o*-iminobenzoquinone[6] for **1**; Q = $^{O,O}Q^0$ = 3,5-di-*tert*-butyl-*o*-benzoquinone for **3**; Scheme 1).[7]

The synthesis and electrochemical and spectroscopic properties of these complexes have been reported by us in recent years.[7] In an initial report, we showed that the otherwise inert complex **1** could be made reactive toward chemical reagents by subjecting it to a reversible, one-electron oxidation process.[7d] Our work, in line with that of other groups,[4c] highlighted the need for an [NR] group on the Q ligand to stabilize the oxidized complex and hence indicate that compound **1** will hold much promise for redox-induced chemical reactivity studies. Complexes **1** and **3** show strong absorption in the vis–near-IR (NIR) region [Figures S1 and S2 in the Supporting Information (SI); see the discussion below]. The donor–acceptor motif enables light-induced charge transfer with the potential to form a charge-separated state, as observed in other

Received: September 30, 2013
Published: January 8, 2014

   dx.doi.org/10.1021/ic4024713 | *Inorg. Chem.* 2014, 53, 1021–1031

Scheme 1. Ligands pap, $^{O,N}Q^{2-}$, and $^{O,O}Q^{2-}$ and Complexes 1a, 1b, and 3

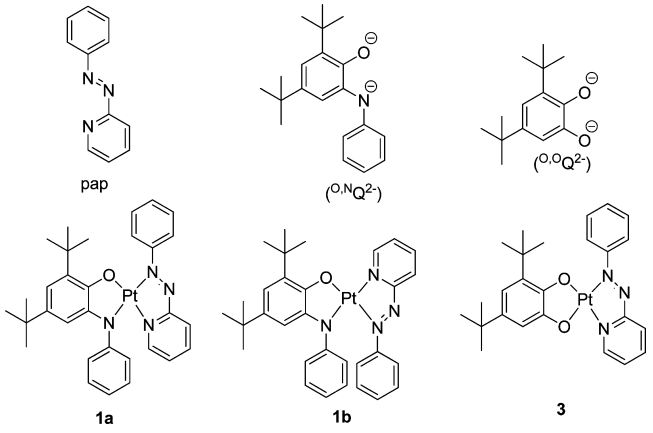

platinum(II) diimine catecholate systems.[1e,f] These states could be perceived as involving a one-electron-oxidized catecholate/amidophenolate unit, just as will be observed upon one-electron oxidation of the parent compound. These compounds also offer an opportunity to directly compare the nature and dynamics of the excited states in catecholate versus amidophenolate complexes, as well as between Pt^{II}pap complexes and those containing a diimine such as 2,2′-bipyridine in place of pap. The present study is aimed at the following questions:

(1) What are the geometric and electronic structural features of the one-electron-oxidized form of **1**?

(2) How does redox-induced reactivity in **1** work and what is its mechanism?

(3) What kinds of products are formed in the reaction of the one-electron-oxidized form of **1** with nucleophiles?

(4) What is the nature of the excited states of **1** and **3** and what is the influence of the change in the nature of the donor ligand, from catecholate to an amidophenolate, on the nature and dynamics of the lowest excited state?

In the following, we present results from synthesis, electrochemistry, UV−vis−NIR, and electron paramagnetic resonance (EPR) spectroelectrochemistry, and time-resolved infrared (TRIR) spectroscopy to address these questions. We further report the results from simulations of cyclic voltammogram and density functional theory (DFT) calculations. Finally, we apply the recently introduced metrical oxidation state (MOS) concept to elucidate and compare the results for the compounds presented here with platinum(II) diimine catecholate complexes.

RESULTS AND DISCUSSION

Synthesis and Crystal Structures. Compound **1** was synthesized by a procedure reported by us recently using $Pt(pap)Cl_2$[7a] and $H_2{}^{O,N}Q$ in the presence of a base.[7d] **1** can be obtained in high yield and purity by using this route, and hence large amounts of this compound can be easily synthesized for investigating its chemical reactivity. As we had reported earlier, complex **1** is unreactive toward tested external substrates such as H_2, PPh_3, and pyridine and is stable as a solid and in solution under ambient conditions.[7d] The reactivity in **1** is switched on by performing one-electron oxidation of this complex. Because the one-electron-oxidized form of **1** is the reactive species that can be used as a precursor for a diversity of compounds in electrochemical synthesis,[7d] chemically isolating this compound and determining its structure by single-crystal X-ray diffraction studies is of considerable interest. **1** was cleanly oxidized by reaction with 1 equiv of $AgBF_4$ in CH_2Cl_2 and subsequent recrystallization to generate $[\mathbf{1}]BF_4$ in reasonable yields (Scheme 2 and the Experimental Section).

Scheme 2. Chemical Oxidation Reaction of 1 (Top) and the Two Possible Positional Isomers of 1 (Bottom); See Text for an Explanation

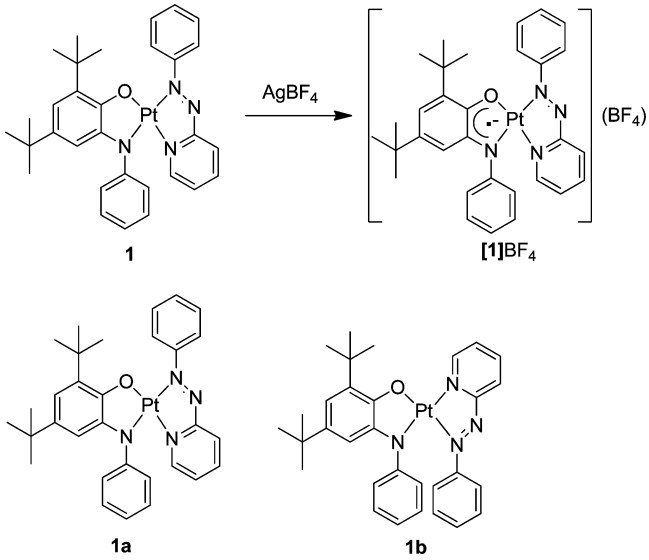

Single crystals of $[\mathbf{1}]BF_4$ were obtained by layering a dichloromethane solution with pentane. $[\mathbf{1}]BF_4$ crystallizes in the monoclinic *Cc* space group (Table S1 in the SI). The Pt center in $[\mathbf{1}]BF_4$ is in a slightly distorted square-planar environment, being coordinated by the O and N donors of one ligand and two N donors of the other ligand (Figure 1).

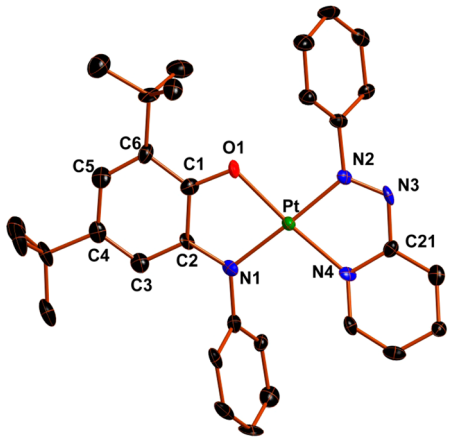

Figure 1. Perspective view of $[\mathbf{1}]BF_4$. Ellipsoids are drawn at 50% probability. H atoms and counterions have been omitted for clarity.

Because both the ligands have two different donors each, the synthesis of **1** had delivered a mixture of two positional isomers [azo N of pap trans to either N (**1a**) or O (**1b**) of $^{O,N}Q$].[7d] For the neutral compound, we were able to crystallize the isomer **1b**, and bond-length analysis had established this complex as $[(^{O,N}Q^{2-})Pt(pap^{0})]$ with strong π delocalization between $^{O,N}Q^{2-}$ and pap.[7d] Several attempts at obtaining single crystals

dx.doi.org/10.1021/ic4024713 | Inorg. Chem. 2014, 53, 1021−1031

of the oxidized form of **1b** were not successful. Hence, we turned our attention to the oxidized form of **1a** (for the rest of the text (except for the TRIR section) the compounds will be called **1** and [**1**]BF_4 for simplification. This is justified because the electrochemical and UV−vis−NIR spectroscopic properties of the two isomers are identical). Upon moving from **1** to [**1**]BF_4, the C1−O1 bond length changes from 1.329(4) to 1.227(9) Å, and the C2−N1 bond length changes from 1.386(5) to 1.31(1) Å. The shortening of these two bonds is in line with oxidation taking place predominantly on the $^{O,N}Q$ ligand. A look at the intraring bond lengths of $^{O,N}Q$ in [**1**]BF_4 shows alternation of the C−C bond lengths in comparison to **1**, where these bonds are more averaged (Table S2 in the SI).[2g,8] All of the bond lengths within the $^{O,N}Q$ ligand, together with the total charge of 1+ in [**1**]BF_4, points to the best formulation of this compound as [($^{O,N}Q^{\bullet-}$) Pt(pap^0)](BF_4).

Recently, a new concept called the MOS has been introduced in the literature for determining the oxidation level of noninnocent ligands such as catecholates and amidophenolates.[9] This concept, which takes all of the relevant C−C, C−O, and C−N bond lengths of such ligands into consideration for calculating MOS, is a convenient way of quantifying the structural results and correlating them to "formal" ligand oxidation states. Furthermore, such an analysis also provides valuable insight into the actual bonding situation in metal complexes of such noninnocent ligands. For **3**, the value of MOS for the ligand $^{O,O}Q$ is −1.9, and this fits perfectly well with the description of **3** as [($^{O,O}Q^{2-}$)Pt(pap^0)]. For related complexes [(Q^{2-})Pt(bpy^0)] [Q^{2-} = substituted catecholate or amidophenolate and bpy = (substituted) 2,2′-bipyridine], the MOS values for Q are always close to −2.[2a−c,g,9] However, the MOS value for $^{O,N}Q$ in **1** is −1.5. This value is certainly smaller than the value of −2 expected for an amidophenolate ligand. Amidophenolates are known to engage in better π-bonding interactions compared to their catecholate counterparts, hence resulting in noninteger oxidation states for these ligands, particularly in combination with relatively electron-poor metal centers.[9] An important and interesting question here is, how does this concept apply to platinum(II) complexes? The answer to this question lies in analysis of the bond lengths within the pap ligand. For **1**, the azo bond N2−N3 has a length of 1.321(4) Å, whereas for **3**, this bond length is 1.307(7) Å. In such donor−acceptor systems, the donor ligands such as $^{O,N}Q$ or $^{O,O}Q$ are capable of π donation into the low-lying π^* orbitals of the pap acceptor. As has been mentioned above, ligands of the type $^{O,N}Q$ are better at undergoing π donation than $^{O,O}Q$. π-Back-donation into the pap ligand would result in an elongation of the azo N═N bond. For the complex containing $^{O,N}Q$, this elongation is expected to be greater than that in the complex containing $^{O,O}Q$. This is exactly what is observed in **1** compared to **3**. Similar effects in other bond lengths of pap are also observed (Table S2 in the SI). It is this π donation in **1** that leads to noninteger MOS. Although such an effect is well established for a metal complex with titanium(IV) or vanadium(V),[9] it is fascinating that these effects can also be observed in a complex containing platinum(II). The reason for this occurrence is the strongly π-accepting ligand pap that is present in this complex, implying an effective platinum(II)-mediated communication between the donor and acceptor ligands. To the best of our knowledge, the MOS value of −1.5 for amidophenolates is one of the lowest values observed in combination with relatively electron-rich metal centers such as Pt^{II}. Thus, even though the limiting description of [($^{O,N}Q^{2-}$)-Pt(pap^0)] for **1** works reasonably well for most purposes, it is important to note the extensive electron delocalization from $^{O,N}Q^{2-}$ to pap, leading to noninteger oxidation states for these ligands and showing the need for invoking forms such as [($^{O,N}Q^{(2-n)-}$)Pt(pap^{n-})] (n = noninteger < 1) to describe the real bonding situation in these complexes.

The calculated MOS of $^{O,N}Q$ for the oxidized complex [**1**]BF_4 is −0.91, and this value is exactly what is expected for the iminosemiquinone form of this ligand. Oxidation to iminosemiquinone drastically reduces the π-donating character of $^{O,N}Q$, and hence almost an integer value for MOS is obtained for this case. Accordingly, the N2−N3 bond length of pap has a value of 1.25(1) Å, indicating negligible π donation to pap, as would be expected for a relatively electron-poor iminosemiquinone ligand. Thus, [($^{O,N}Q^{\bullet-}$)Pt(pap^0)](BF_4) is a near-perfect description for [**1**]BF_4.

We had observed the reaction of $\mathbf{1}^+$ with PPh_3 while performing cyclic voltammetric experiments.[7d] This reaction can be taken as a model for the redox-induced reactivity of **1** in general, and hence unravelling its mechanism is of broad interest. The mechanism of this process has now been analyzed in depth (see below). Our initial studies had shown the formation of a species of the form [($^{O,N}Q^{\bullet-}$)Pt(pap^0)PPh_3]$^+$ upon reaction of the chemically isolated [($^{O,N}Q^{\bullet-}$)Pt(pap^0)]$^+$ with PPh_3. Evidence for this species was gathered from in situ mass spectrometric and EPR spectroscopic studies (Figure S3 in the SI), which showed hyperfine coupling to ^{14}N, ^{1}H, and ^{31}P nuclei. In order to understand the nature of the species formed in the reaction between the oxidized species and PPh_3, crystals suitable for X-ray diffraction studies were obtained. **1** was oxidized with 1 equiv of $AgPF_6$, and the precipitated Ag^0 was removed. PPh_3 was then added to this solution, and the reaction mixture was left to crystallize (see the Experimental Section), yielding compound [**2**]PF_6. [**2**]PF_6 crystallizes in the triclinic $P\bar{1}$ space group (Table S1 in the SI). The Pt center is in a distorted square-planar environment and is coordinated through the O and N atoms of $^{O,N}Q$ and through the P atoms of two PPh_3 ligands (Figure 2). Thus, reaction of the one-electron-oxidized form [**1**]PF_6 with PPh_3 in solution at room temperature leads to substitution of the pap ligand by two PPh_3 ligands, forming [**2**]PF_6. The reason for this is likely the better donor ability of PPh_3 in comparison to that of pap. We believe

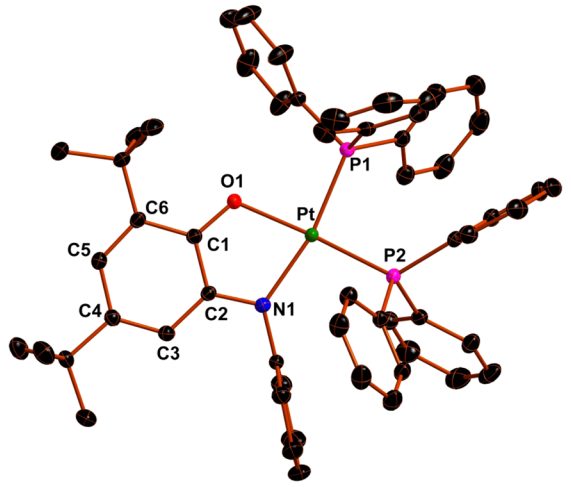

Figure 2. Perspective view of (**2**)PF_6. Ellipsoids are drawn at 50% probability. H atoms and counterions have been omitted for clarity.

dx.doi.org/10.1021/ic4024713 | Inorg. Chem. 2014, 53, 1021−1031

that the formation of 2^+ proceeds through the species $[(^{O,N}Q^{\bullet-})Pt(pap^0)PPh_3]^+$ because this is the initial species detected immediately after reacting 1^+ with PPh_3. 2^+ is thus the most thermodynamically stable product. The Pt−P bond lengths are within the range expected for Pt^{II}−P bonds (Table S2 in the SI). The bond lengths within the $^{O,N}Q$ ligand fit quite well with those of $[1]BF_4$ and with what is expected for the iminosemiquinone ($^{O,N}Q^{\bullet-}$) form of this ligand (Table S2 in the SI). Thus, $[2]PF_6$ is best described as $[(^{O,N}Q^{\bullet-})Pt(PPh_3)_2](PF_6)$. The calculated MOS value for this complex is −1.06 and justifies the description given above. The iminosemiquinone form is electron-poor, and the complex $[2]PF_6$ does not have π-accepting ligands. Hence, the iminosemiquinone form is an adequate description for $^{O,N}Q$ in $[2]PF_6$.

Cyclic Voltammetry. The electrochemical data on **1** and **3** reported previously are briefly summarized here for comparison purposes.[7b,d] In the case of **1**, which has an isoelectronic NR group on $^{O,N}Q^{2-}$ instead of O, the redox potentials are significantly different from those of **3**. The more electron-donating amidophenolate ligand ($^{O,N}Q^{2-}$) leads to a cathodic shift of the oxidation potentials of **1** compared to those of **3** (Table 1) of more than 0.2 V. The chemical reversibility of the second oxidation process improves on going from **3** to **1**. This observation is related to the better donating ability of the completely oxidized *o*-iminoquinone form, and hence its ability to bind better to a metal center, compared to its all-oxygen-donating counterparts, the *o*-quinones. Remarkably, the first reduction potential for **1** is also shifted by about 250 mV compared to that for **3**. This process, which takes place predominantly on the pap ligand, is clearly influenced by the nature of the donor ligands in the complexes, indicating electronic communication through the metal center. As has been discussed above, the significant π donation from $^{O,N}Q^{2-}$ to pap results in this large cathodic shift of the first reduction potential on moving from **3** to **1**. As can be seen in Table 1, the influence of changing the donor ligand on the second reduction potential of the complexes is significantly smaller compared to their influence on the first reduction potential.

Table 1. Electrochemical Data from Cyclic Voltammetry[a]

compound	E^{ox2} (V)	E^{ox1} (V)	E^{red1} (V)	E^{red2} (V)	ΔE^{neu} (V)[b]
1[c]	0.60	−0.09	−1.19	−1.73	1.10
2(PF_6)		0.33	−0.54		0.87
3[d]	0.93[e]	0.12	−0.94	−1.75	1.06

[a]Half-wave potentials from cyclic voltammetric measurements in CH_2Cl_2/0.1 M Bu_4NPF_6 for reversible processes at 298 K with a scan rate of 100 mV s^{-1}. Ferrocene/ferrocenium was used as the internal standard. [b]$\Delta E^{neu} = E^{ox1} - E^{red1}$. [c]From ref 7d (values have been corrected). [d]From ref 7b. [e]E_{pa} for the irreversible process.

Complex **1**, which is stable with respect to reactions with tested external substrates such as H_2 and PPh_3, can be activated toward such reactions by one-electron oxidation. A simulation of the cyclic voltammogram of **1** in the presence of PPh_3 was performed in order to gain insight into the mechanism of this process; the resulting curve fits the experimental data well (Figure 3). The overall process can be described by a cyclic electron transfer/chemical reaction/electron transfer/chemical reaction (ECEC) mechanism, as shown in Scheme 3, where the best-fit parameters for the various steps are also given.

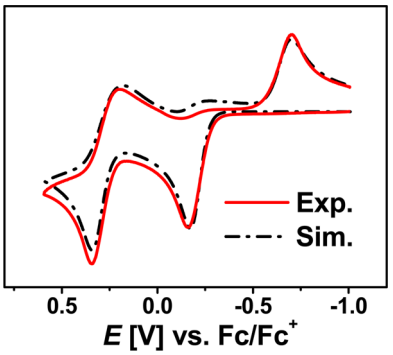

Figure 3. Cyclic voltammogram of a solution of **1** and PPh_3 (solid red line)[7d] and simulation (dashed black line). Conditions: CH_2Cl_2, 0.16 × 10^{-3} M **1**, 0.16 M PPh_3, 0.1 M Bu_4NPF_6, and a scan rate of 100 mV s^{-1}.

The initial one-electron oxidation at E_1 = −0.16 V activates the complex for its reaction with PPh_3. The cationic complex then reacts with PPh_3 to form the complex $[Pt(pap^0)(^{O,N}Q^{\bullet-})(PPh_3)]^+$. The equilibrium constant for this process is on the order of 10^8 M^{-1}, and the rate of the forward reaction is about 10^8 orders of magnitude faster compared to that of the back-reaction. These parameters point to the facile formation of $[Pt(pap^0)(^{O,N}Q^{\bullet-})(PPh_3)]^+$ upon performing one-electron oxidation of **1**. The identity of $[Pt(pap^0)(^{O,N}Q^{\bullet-})(PPh_3)]^+$ was also established in in situ mass spectrometric and EPR spectroscopic studies (Figure S3 in the SI).[7d] The species $[Pt(pap^0)(^{O,N}Q^{\bullet-})(PPh_3)]^+$ can be reversibly oxidized in a one-electron step at E_2 = 0.27 V to $[Pt(pap^0)(^{O,N}Q^0)(PPh_3)]^{2+}$. The rate of electron transfer for this step is slower in comparison to that of the first step (Scheme 3) possibly because of the increase in the total charge of the complex and the resulting Coulombic interactions. The species $[Pt(pap^0)(^{O,N}Q^{\bullet-})(PPh_3)]^+$ formed upon re-reduction of $[Pt(pap^0)(^{O,N}Q^0)(PPh_3)]^{2+}$ is then reduced in an one-electron step at E_3 = −0.70 V to form $[Pt(pap^0)(^{O,N}Q^{2-})(PPh_3)]$. The thus-formed complex $[Pt(pap^0)(^{O,N}Q^{2-})(PPh_3)]$ is unstable and dissociates spontaneously to form **1** and PPh_3. The equilibrium constant for this reaction is on the order of 10^6 M, and the rate of the forward reaction is 10^7 order of magnitude faster than the back-reaction. These observations are in line with the unreactive nature of the neutral complex **1** toward external substrates. The overall mechanism is thus a chemically reversible cyclic ECEC process. Upon a decrease in the temperature to −40 °C, the nature of the cyclic voltammograms measured in the presence of PPh_3 changes (Figure S4 in the SI). This is likely a result of the lower reaction rates of the chemical reactions that follow the redox processes. Association/dissociation of PPh_3 to the oxidized complex is expected to be slower at lower temperatures, and the lower rates of those reactions will ensure the presence of a higher number of redox-active species on the cyclic voltammetric time scale (for instance, incomplete dissociation of PPh_3 from the aforementioned five-coordinate platinum complex). As a result of this, the number of redox steps observed at lower temperatures is higher.

As has been pointed out in the section on the synthesis, complex $1^{\bullet+}$ slowly reacts with PPh_3 in solution, forming a new complex, $[2]PF_6$, as the most thermodynamically stable product. It should be noted here that the synthesis of complexes such as $[2]PF_6$ through conventional synthetic routes is difficult, and to the best of our knowledge, only few

dx.doi.org/10.1021/ic4024713 | Inorg. Chem. 2014, 53, 1021−1031

Scheme 3. Parameters Used in the Simulation of the Voltammogram of 1 in the Presence of PPh_3 and Proposed ECEC Mechanism for Coordination of PPh_3 to 1^+

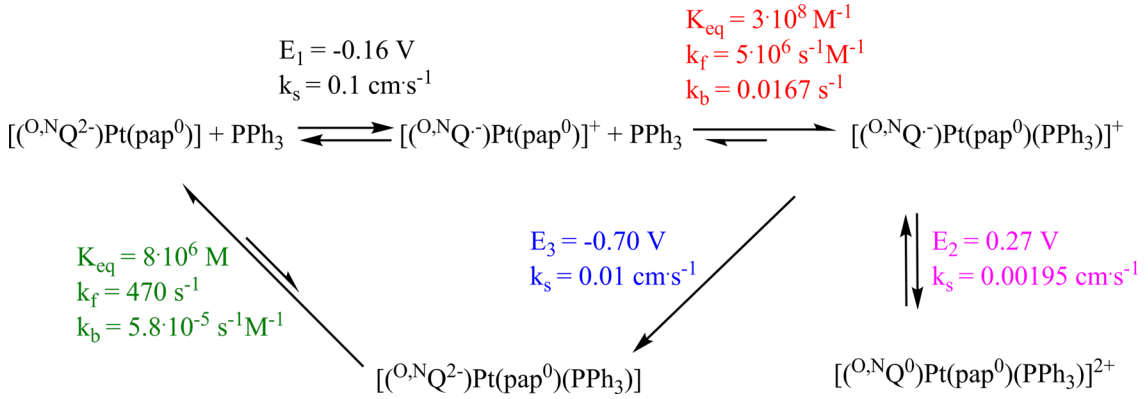

examples of such complexes are known.[10] [**2**]PF_6 can be reversibly oxidized and reduced in one-electron steps (Figure 4 and Table 1).

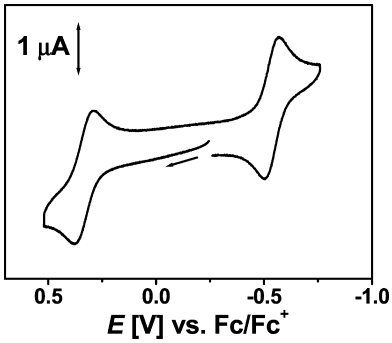

Figure 4. Cyclic voltammogram of 2^+ in CH_2Cl_2/0.1 M Bu_4NPF_6 at 295 K. Scan rate: 100 mV s^{-1}.

From structural analysis, [**2**]PF_6 was established as $[(^{O,N}Q^{\bullet-})Pt(PPh_3)_2](PF_6)$. Thus, one-electron oxidation is expected to result in $[(^{O,N}Q^{0})Pt(PPh_3)_2]^{2+}$ and one-electron reduction in $[(^{O,N}Q^{2-})Pt(PPh_3)_2]$. Hence, it is seen that the stability of the $^{O,N}Q^{2-}$ form decreases on changing from **1** to [**2**]PF_6. This effect is related to the coligands present in the two complexes. The pap ligand present in **1** is a strong π acceptor and is hence capable of better stabilizing the electron-rich $^{O,N}Q^{2-}$ in **1**. On the contrary, PPh_3 is a strongly donating ligand, which leads to the increased propensity of $^{O,N}Q^{2-}$ to get oxidized to $^{O,N}Q^{\bullet-}$, the form seen to be stabilized in [**2**]PF_6.

UV–Vis–NIR and EPR Spectroscopy and Spectroelectrochemistry. The neutral complexes **1** and **3** each display an intense absorption band in the NIR region (Figure 5 and Table S3 in the SI), which can be attributed to the combination of a Q^{2-}-to-pap ligand-to-ligand charge-transfer (LLCT) transition with a Pt^{II}-to-pap metal-to-ligand charge-transfer (MLCT) transition.[7b,d] In view of the discussion on the crystal structures presented above, **3** is likely to have more charge-transfer character in this NIR band. For **1**, because there is substantial delocalization in the ground state of the molecule, a charge-transfer description is less applicable. In agreement with this hypothesis, the lowest-energy absorption band of **3** displays a strong negative solvatochromism with absorption maxima of 1011 and 1114 nm in CH_2Cl_2 and *n*-hexane, respectively (914 cm^{-1}). The absorption maximum of this charge-transfer band

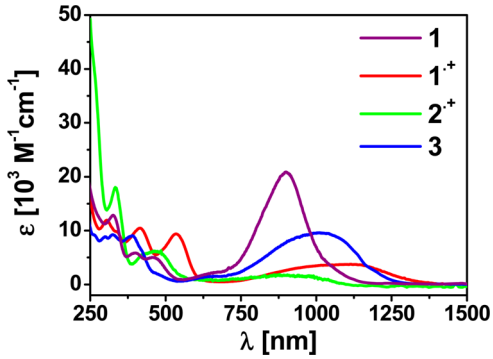

Figure 5. UV–vis–NIR spectra of complexes in CH_2Cl_2.

expressed in reciprocal centimeters shows a linear dependence on the solvent polarity, as can be seen from Figure S1 in the SI.[11,2a] In contrast to **3**, the solvent dependence of the lowest-energy absorption band for **1** is negligible (Figure S2 in the SI). The bandwidths of the lowest-energy bands for both complexes also display solvent dependence. However, the dependence of the width on the solvent polarity is opposite for the two complexes (Figures S1 and S2 in the SI). The position of the NIR bands in these neutral complexes correlates well with the difference between the potentials of the first oxidation and first reduction steps (Table 1), appearing at 897 nm for **1** and at 970 nm for **3**.

One-electron oxidation of **1** in an optically transparent thin-layer electrochemical (OTTLE) cell leads to a loss of intensity of the initial NIR band and a shift to longer wavelengths (1114 nm). The band at 415 nm, which appears for $\mathbf{1}^{\bullet+}$, is typical for an iminosemiquinonato ligand.[7d] Furthermore, there is a band at 535 nm for $\mathbf{1}^{\bullet+}$ that can be tentatively assigned to a MLCT transition. Because [**2**]PF_6 has been convincingly assigned as $[(^{O,N}Q^{\bullet-})Pt(PPh_3)_2](PF_6)$, it is worthwhile to compare its UV–vis–NIR spectroscopic signatures to those of $\mathbf{1}^{\bullet+}$. $\mathbf{2}^{\bullet+}$ displays absorptions in the vis–NIR region at 908, 469, and 421 nm (Table S3 in the SI and Figure 5). These bands are reminiscent of the bands observed for $\mathbf{1}^{\bullet+}$. Particularly, the band at 421 nm is an indication of the presence of an iminosemiquinonato radical ligand in $\mathbf{2}^{\bullet+}$. Thus, both $\mathbf{1}^{\bullet+}$ and $\mathbf{2}^{\bullet+}$ clearly contain the $^{O,N}Q^{\bullet-}$ form of the ligand, as has also been discussed in the structural part above. The bands in the UV region can be assigned to transitions within the ligands.

One-electron oxidation of $\mathbf{2}^{\bullet+}$ to $\mathbf{2}^{2+}$ leads to the disappearance of the initial bands in the NIR region. In the

dx.doi.org/10.1021/ic4024713 | Inorg. Chem. 2014, 53, 1021–1031

visible region, a new band appears at 593 nm (Figure 6), and this band is assigned to a MLCT transition corresponding to

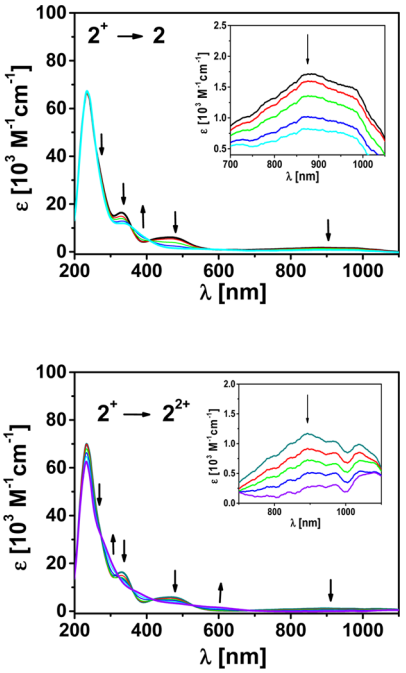

Figure 6. Changes in the UV−vis−NIR spectrum of $\mathbf{2}^{+}$ during OTTLE spectroelectrochemistry in CH_2Cl_2/0.1 M Bu_4NPF_6. Inset: zoomed part of the NIR region.

the formulation $[(^{O,N}Q^{0})Pt(PPh_3)_2]^{2+}$. One-electron reduction to **2**, on the other hand, makes the compound completely transparent in the visible and NIR regions, as would be expected for the formulation $[(^{O,N}Q^{2-})Pt(PPh_3)_2]$ with a completely reduced amidophenolate ligand without any other acceptor ligand in that molecule.

The paramagnetic complex $\mathbf{2}^{\bullet+}$ was also studied by EPR spectroscopy. At 295 K in CH_2Cl_2, $\mathbf{2}^{\bullet+}$ exhibits an EPR signal centered at g = 1.999 (Figure 7). This signal could be simulated

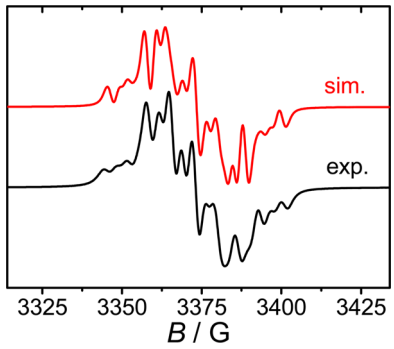

Figure 7. X-band EPR spectrum of $(\mathbf{2})PF_6$ in CH_2Cl_2 at 295 K (bottom) and the corresponding simulated spectrum (top).

by considering hyperfine coupling constants of 3.2, 7.7, and 6.4 G (5.4 G for two different P nuclei) respectively to ^{1}H (I = $^{1}/_{2}$), ^{14}N (I = 1), and ^{31}P (I = $^{1}/_{2}$) nuclei.[12] Additionally, platinum satellites (^{195}Pt, I = $^{1}/_{2}$, and natural abundance = 33.3%) of 23.2 G were also taken into consideration for the simulation. The appearance of the signal at room temperature in a fluid solution and the g value are an indication of predominantly ligand-centered spin. Furthermore, the hyperfine coupling constants calculated for the ^{1}H and ^{14}N nuclei are typical for the iminosemiquinonato ligand. These data thus point to the predominant spin localization on the iminosemiquinonato ligand in $\mathbf{2}^{\bullet+}$. Spin polarization also leads to the observation of hyperfine coupling to the ^{31}P and ^{195}Pt nuclei, albeit with very small coupling constants to these nuclei, which are otherwise known to exhibit large hyperfine coupling constants.

Fourier Transform Infrared (FTIR) and TRIR Studies. In order to investigate the dynamics of the excited states in such delocalized systems, compare catecholate versus aminophenolate behavior, and compare the behavior of the Pt(pap) compound with those of the Pt(diimine) type, picosecond TRIR studies have been undertaken.

The FTIR spectra of **1b** and **3** (Figure 8) show a number of bands in the fingerprint region. The band assignments obtained

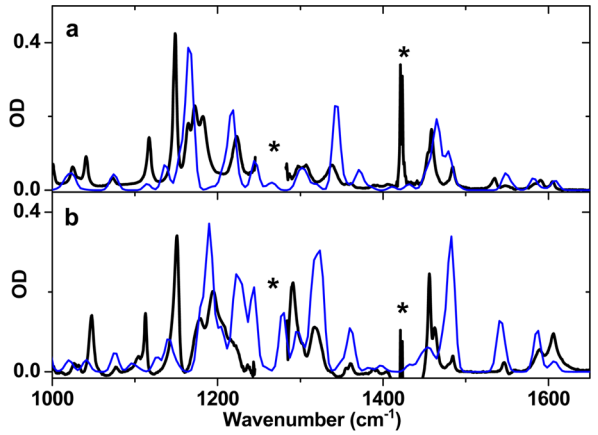

Figure 8. FTIR spectra of (a) **1b** and (b) **3** in CH_2Cl_2 at room temperature. Calculated spectra are shown in blue. Asterisks indicate regions of strong solvent absorbency.

from DFT calculations are given in the SI (Figures S5−S8 and Tables S4−S7). The ground-state IR absorptions for both compounds are dominated by ring-bending modes at 1460−1480 cm^{-1} (phenyl and pyridine rings) coupled to the catecholate ring and −CH bending modes of the ^{t}Bu groups of the catechol, and by catecholate ring-bending modes at 1530−1550 cm^{-1} (Tables S4−S7 in the SI). DFT calculations show that these are strongly coupled throughout the molecule for both complexes, in both the singlet and triplet ground states.

The picosecond TRIR spectra in the 1420−1620 cm^{-1} region following 400 nm excitation for **1b** and **3** in CH_2Cl_2 are shown in Figure 9. 400 nm excitation leads to an instant bleaching of the ground-state bands and to the formation of several transient bands that decay to the baseline on a variety of time scales (vide infra). We note that DFT calculations find a considerable platinum contribution into the frontier orbitals, which may lead to an ultrafast intersystem crossing in the initially populated singlet excited state.[13] Thus, it is likely that the electronically excited state(s) detected by TRIR on the time scale of >5 ps will be in the triplet manifold. Accordingly, the IR spectra of the lowest triplet states were obtained with DFT calculations for comparison with the TRIR data.

For **1b**, $[(^{O,N}Q^{2-})Pt(pap^{0})]$, two distinct processes can be observed: a fast, 4.7 ± 0.9 ps lifetime component appears as broad signals throughout the spectra (inset of Figure 9B), while

dx.doi.org/10.1021/ic4024713 | Inorg. Chem. 2014, 53, 1021−1031

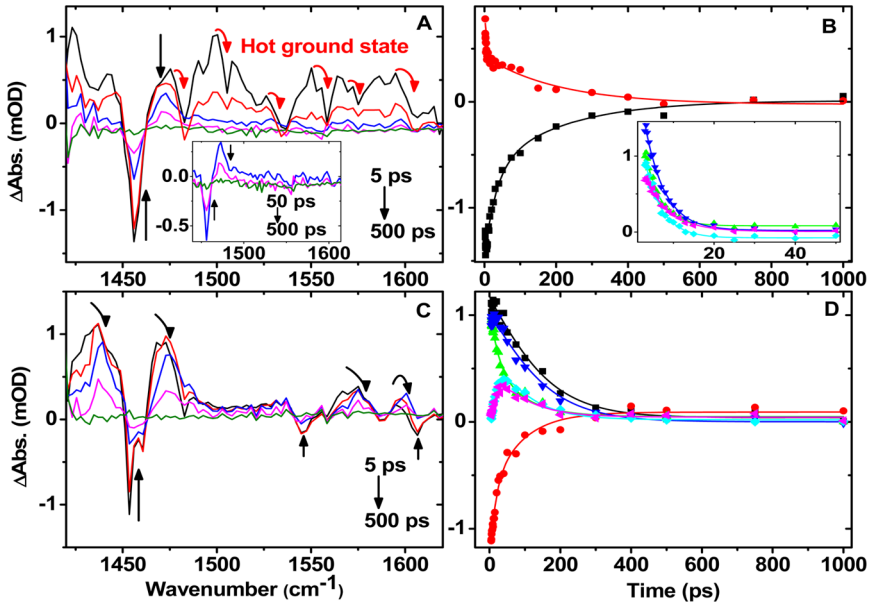

Figure 9. TRIR spectra and corresponding kinetic traces for compounds **1b** (A and B) and **3** (C and D) in CH_2Cl_2. Inset in A: spectra at late times, once hot ground-state signals have disappeared. In B and D, symbols represent single-pixel kinetics from the raw data; lines correspond to double-exponential best fits. Kinetic traces are at 1456, 1473, 1490, 1500, 1550, and 1595 cm^{-1} (B, with the last four shown in the inset with expanded scale) and at 1437, 1454, 1468, 1473, 1483, and 1601 cm^{-1} (D) (black, red, green, blue, cyan, and magenta, respectively).

a longer, 190 ± 20 ps lifetime persists at two positions only, the ground state bleach at 1456 cm^{-1} and the transient at 1473 cm^{-1}. These latter bands correspond to delocalized bending modes of the pyridine and phenyl rings. This observation points to several important conclusions. First, the nature of the lowest excited state in **1b** (the 190 ps process), which possesses an amidophenolate ligand, is mainly an intra-pap (intraligand triplet, ^{3}IL) state rather than a charge-transfer state. This conclusion is consistent with the relatively small solvatochromism of the lowest-energy electronic absorption band in this compound compared to **3** and to other platinum(II) catecholates.[14] Second, the fast process appears as anharmonically shifted ground-state bands, which are characteristic of "hot", vibrationally excited ground states that are formed because of very fast energy loss from the higher-lying electronic excited state on time scales of less than 5 ps after initial excitation.[13,14−17] This result implies that the ultrafast nonradiative deactivation of the initially formed excited state to the ground state is efficient and therefore that the yield of the excited state is relatively low.

The excited-state dynamics of **3** also involve two decay components on time scales longer than 5 ps. A 23 ± 2 ps component is observed as a shift of spectral signals toward higher energy as the bands decay, as indicated by the arrows in Figure 9C. This behavior on such time scales is characteristic of a vibrational cooling process observed as the vibrationally hot electronic excited states equilibrate with the surrounding solvent.[15,2c] This is shown as "grow-in" kinetic components at some spectral positions, which reflects a shift to higher frequencies as cooling occurs. A longer component with a 140 ± 15 ps lifetime is observed as transients and ground-state bleaches throughout the region of interest and uniformly decays down to the baseline. Thus, in the case of **3** and differently to **1b**, several pairs of ground-state bleaches/transient signals are observed that involve both pap and catecholate vibrations, albeit highly delocalized. These observations lead to the assignment of an electronic excited state in **3** as pap/Pt-to-Pt/catecholate charge transfer (^{3}CT) in nature. This assignment is consistent with the displayed strong solvatochromic behavior of **3** and is typical of Pt(diimine)(catecholates).[2b] The lifetimes of the lowest excited states in **1b** and **3** are of the same order of magnitude as those previously reported for several mononuclear and dinuclear Pt(diimine)(catechols): 420 and 630 ps for [Pt(bpyam)(^{O,O}Q)] and [Pt(^{t}Bu$_2$bpy)(^{O,O}Q)], respectively, and 690 and 285 ps for the binuclear {Pt(^{t}Bu$_2$bpy)}$_2$(biscat) and {Pt(bpyam)}$_2$(biscat), where bpyam = 4,4′-(CONEt$_2$)$_2$-2,2′-bipyridine, ^{t}Bu$_2$bpy = 4,4′-di-*tert*-butyl-2,2′-bipyridine, and biscat = tetraanion of 3,3′,4,4′-tetrahydroxybiphenyl.[2c]

A summary of the TRIR-deduced photophysical pathways for **1b** and **3** following 400 nm excitation is shown in Scheme 4.

DFT Calculations of Frontier Orbitals and Spin Density. In order to verify the composition of the frontier orbitals of complex **1** in the ground state and to determine the spin-density distribution of the one-electron-oxidized and -reduced states of this complex, DFT calculations were carried out with the program *ORCA* for complex **1**. Similar calculations

Scheme 4. Summary of the Photophysical Pathways Observed in TRIR Experiments for 1b (Left) and 3 (Right) in CH_2Cl_2 Following 400 nm Excitation

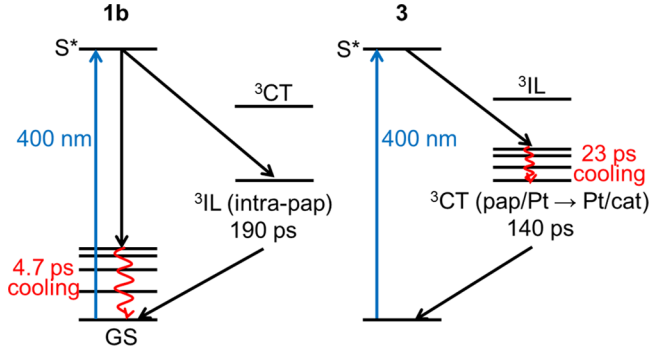

dx.doi.org/10.1021/ic4024713 | Inorg. Chem. 2014, 53, 1021−1031

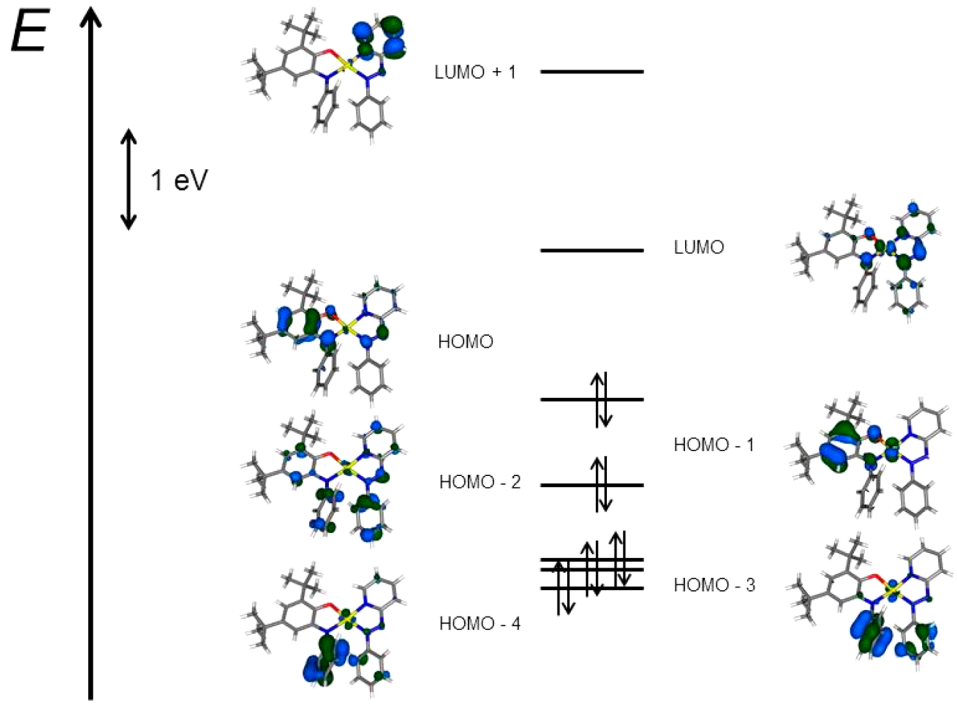

Figure 10. Molecular orbital scheme of the native form. Canonical orbitals (B3LYP).

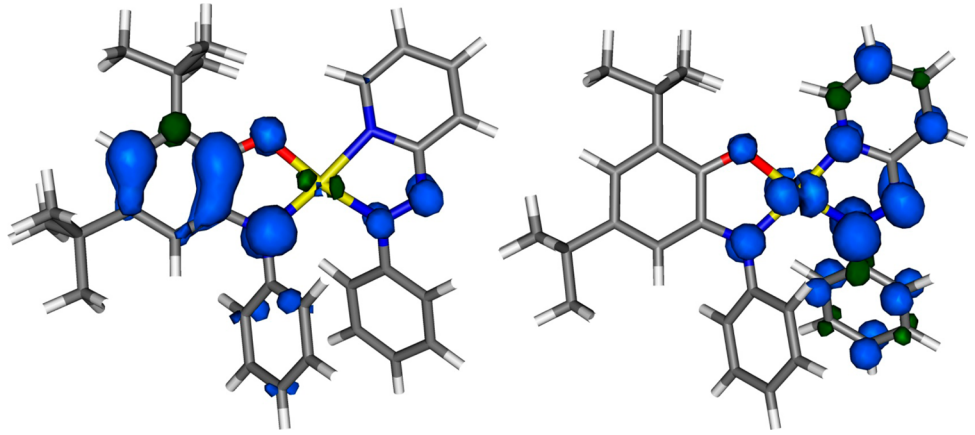

Figure 11. Spin-density distribution of $\mathbf{1}^{\bullet+}$ (left) and $\mathbf{1}^{\bullet-}$ (right).

on **3** have been reported by us previously.[7c] As can be seen from Figure 10, the frontier orbitals of **1** are composed mainly of combinations of orbitals from the $^{O,N}Q^{2-}$ and the pap ligand. The Pt^{II} center makes only a negligible contribution to these frontier orbitals.

$^{O,N}Q^{2-}$ is seen to make the predominant contribution to the highest occupied molecular orbital, with a small orbital coefficient observed in the pap ligand. For the lowest unoccupied molecular orbital, the orbital coefficients are highest on the azo N atoms of the pap ligand. These results confirm the predominant contribution of the redox-active ligands to the frontier orbitals of complex **1**.

Spin-density distribution and EPR parameters were calculated for the one-electron-oxidized, as well as the one-electron-reduced, forms of **1**. The calculated g values and hyperfine coupling constants to all nuclei (except Pt) are reproduced with reasonable accuracy with these calculations. As can be seen from Figure 11, for $\mathbf{1}^{\bullet+}$, the spin density is largely localized on the $^{O,N}Q$ ligand, as would be expected for the formulation $[(^{O,N}Q^{\bullet-})Pt(pap^{0})]^{+}$; the calculated parameters are g = 1.979, $a(^{195}Pt)$ = −76.0 G, $a(^{14}N)$ = 5.3 G, and $a(^{1}H)$ = −4.7 G [exp: g = 1.988, $a(^{195}Pt)$ = 25.3 G, $a(^{14}N)$ = 6.1 G, and $a(^{1}H)$ = 4.4 G]. For comparison, the experimentally determined $a(^{195}Pt)$ for $\mathbf{3}^{\bullet+}$ is 24 G.

For $\mathbf{1}^{\bullet-}$, on the other hand, the spin density is primarily located in the pap ligand, with about 15% spin density on the Pt center; the calculated parameters are g = 2.031 and $a(^{195}Pt)$ = −299 G [exp: g = 2.008 and $a(^{195}Pt)$ = 127 G]. Thus, for $\mathbf{1}^{\bullet-}$, the best formulation is $[(^{O,N}Q^{2-})Pt(pap^{\bullet-})]^{-}$. The hyperfine coupling to the ^{195}Pt nucleus is experimentally found to be larger for $\mathbf{1}^{\bullet-}$ than for $\mathbf{1}^{\bullet+}$. Accordingly, DFT calculations deliver a larger spin density on the Pt center for $\mathbf{1}^{\bullet-}$ compared to $\mathbf{1}^{\bullet+}$. The calculations thus nicely corroborate the experimental data. The hyperfine coupling constant to the ^{195}Pt nucleus is overestimated in the calculations. For $\mathbf{3}^{\bullet-}$, $a(^{195}Pt)$ was experimentally determined to be 102 G. The spin-density calculations thus confirm almost exclusive localization

dx.doi.org/10.1021/ic4024713 | Inorg. Chem. 2014, 53, 1021−1031

of spin on the redox-active ligands for both the one-electron-oxidized and -reduced forms.

CONCLUSIONS

A new series of platinum(II) charge-transfer complexes that combine a pap electron-acceptor ligand with amidophenolate ($^{O,N}Q^{2-}$ in **1**) or catecholate ($^{O,O}Q^{2-}$ in **3**) donors has been synthesized and fully characterized. The concept of MOS, a method to determine the oxidation level of noninnocent ligands such as catecholates and amidophenolates, has been applied to these compounds using an average of all of the intraligand bond lengths. This approach allowed us to obtain further insight into the electronic structure of these compounds and compare them with their platinum(II) diimine analogues. MOS delivers a value of −1.9 for $^{O,O}Q$ in **3** (the limiting value for the catecholate form is −2) and hence supports the description $[(^{O,O}Q^{2-})Pt^{II}(pap^{0})]$. On the contrary, MOS for $^{O,N}Q$ in **1** is −1.5, showing the presence of noninteger oxidation states for the ligands in **1**. This result is a consequence of the presence of both the strongly π-donating $^{O,N}Q^{2-}$ and the strongly π-accepting pap in **1**, which leads to delocalization between $^{O,N}Q^{2-}$ and pap^{0}. As a consequence, the electron density in the ground state of **1** is delocalized across the molecules, which is also confirmed by a negligible solvent-polarity dependence of the lowest-energy absorption band in **1**. In contrast, the lowest-energy absorption band in **3** displays a strong negative solvatochromism, typical for MLCT/LLCT transitions. The radical cation of **1** is highly reactive with respect to reactions with nucleophiles, and the mechanism of this process for the example of a reaction between $\mathbf{1}^{\bullet+}$ and PPh_3 has been proposed. The thermodynamically stable product of the reaction between $\mathbf{1}^{\bullet+}$ and PPh_3 is $[(^{O,N}Q^{\bullet-})Pt(PPh_3)_2]^{\bullet+}$ ($\mathbf{2}^{\bullet+}$), which is formed upon substitution of the acceptor ligand pap with PPh_3. The nature and dynamics of the excited states in **1b** and **3** have been investigated by picosecond TRIR spectroscopy. The results indicate a stronger charge-transfer character in **3**, with the spectroscopic signatures in TRIR similar to those of previously investigate platinum(II) diimine catecholates. The Pt(pap)(amidophenolate) complex **1b**, on the other hand, displays different TRIR behavior, which is indicative of a lowest excited state of a purely pap-based character. Thus, the TRIR excited-state studies correlate well with the conclusions on the nature of the lowest excited state derived from applying the MOS concept.

This study also shows that the MOS concept and a combined electrochemical and spectroelectrochemical approach can be utilized to rationalize chemical reactivity in metal complexes containing redox-active ligands.

EXPERIMENTAL SECTION

General Considerations. Complexes **1** and **3** were prepared according to reported procedures.[7b,d] All other reagents were commercially available and used as received. All solvents were dried and distilled using common techniques unless otherwise mentioned.

Instrumentation. Cyclic voltammetry was carried out in a 0.1 M Bu_4NPF_6 solution using a three-electrode configuration (glassy carbon working electrode, platinum counter electrode, and silver wire pseudoreference electrode) and a PAR VersaSTAT 4 potentiostat. The ferrocene/ferrocenium (Fc/Fc^{+}) couple served as the internal reference. Cyclic voltammetric simulations employed *DigiElch 7* software. EPR spectra in the X band were recorded with a Bruker System EMX. Simulations of EPR spectra were done using the *Simfonia* program. UV−vis−NIR absorption spectra were recorded on an Avantes spectrometer system: Ava Light-DH-BAL (light source), AvaSpec-ULS2048 (UV−vis detector), and AvaSpec-NIR256-2.5TEC (NIR detector). Spectroelectrochemical measurements were carried out using an OTTLE cell.[18] Elemental analysis was performed on a Perkin-Elmer 240 analyzer. Mass spectrometry experiments were carried out on a Bruker Daltronics Mictrotof-Q mass spectrometer. IR experiments were carried out on a THERMO Nicolet 6700 spectrometer.

Synthesis. *[1]BF_4.* Complex **1** (25 mg, 0.037 mmol) and $AgBF_4$ (7.2 mg, 0.037 mmol) were taken together under a nitrogen atmosphere in 10 mL of dry dichloromethane. The reaction mixture was allowed to stir for 1 h. The color of the solution changed from green to deep red. The reaction mixture was filtered through Celite to remove precipitated silver, rinsing with about 5 mL of dichloromethane until the effluent ran colorless. The solvent was removed under reduced pressure, and the resulting red solid was crystallized from 3 mL of dichloromethane layered with 10 mL of pentane. Yield: 14 mg (0.018 mmol, 49%). Anal. Calcd for $C_{31}H_{34}BF_4N_4OPt\cdot 0.5CH_2Cl_2$: C, 47.12; H, 4.39; N, 6.98. Found: C, 47.13; H, 4.36; N, 7.05. HRMS (ESI). Calcd for $C_{31}H_{34}N_4OPt$ ($[M]^{+}$): m/z 673.2423. Found: m/z 673.2369.

[2]PF_6. A Schlenk tube was charged with complex **1** (26 mg, 0.039 mmol), $AgPF_6$ (9.8 mg, 0.039 mmol), and 10 mL of dry dichloromethane. The reaction mixture was stirred for 1 h. The mixture was filtered through Celite to remove precipitated silver, and PPh_3 (20.5 mg, 0.078 mmol) was added to the solution of the oxidized complex. The color of the solution changed from deep red to orange. The solvent volume was concentrated to about 3 mL, and 15 mL of dry pentane was added. The resulting mixture was cooled to −20 °C to yield a red-brown crystalline solid. The product was isolated via filtration. Yield: 31 mg (0.027 mmol, 69%). Anal. Calcd for $C_{56}H_{55}F_6NOP_3Pt$: C, 57.98; H, 4.78; N, 1.21. Found: C, 57.66; H, 5.11; N, 1.46. HRMS (ESI). Calcd for $C_{56}H_{55}NOPPt$ ($[M]^{+}$): m/z 1014.3406. Found: m/z 1014.3388.

Cyclic Voltammetry Experiment in the Presence of PPh_3. Under a nitrogen atmosphere, **1** (5.4 mg, 0.008 mmol) was dissolved in a degassed CH_2Cl_2/0.1 M Bu_4NPF_6 solution (5 mL). A PPh_3 solution (2.11 mg, 0.008 mmol; 1 mL of CH_2Cl_2) was added to the green solution of the complex. After the addition of the PPh_3 solution, a cyclic votammogram was recorded.

TRIR Spectroscopy. Picosecond TRIR studies were performed in the Ultrafast Spectroscopy Laboratory, Rutherford Appleton Laboratory, STFC, UK, ULTRA[19] facility. The IR spectrometer comprised two synchronized 10 kHz, 8 W, 40 fs, and 2 ps titanium sapphire oscillator/regenerative amplifiers (Thales), which pump a range of optical parametric amplifiers (TOPAS). A portion of the 40 fs Ti:S beam was used to generate tunable mid-IR probe light with around 400 cm^{-1} bandwidth. The 400 nm pump beam was generated from the second harmonic of the 40 fs laser. The probe and pump beam diameters in the sample were about 70 and 120 μm, respectively, and the pump energy at the sample was 1 μJ. The pump and probe beams were set at magic angle to each other. In this case, changes in IR absorption spectra were recorded by three HgCdTe linear-IR array detectors on a shot-by-shot basis. The TRIR instrument response was approximately 100 fs. All experiments were carried out in Harrick cells with 2-mm-thick CaF_2 windows with a 390 μm sample path length and a typical optical density of 0.5−1 at 400 nm. All samples were mounted on a 2D-raster stage, and solutions were flowed through the cell to ensure photostability.

DFT Calculations. The program package *ORCA 2.9.1* was used for all calculations.[20] The geometry optimization, frequency analyses, and single-point calculations were performed by the DFT method with BP86 and B3LYP functionals, respectively,[21] including relativistic effects in zero-order regular approximation (ZORA).[22] Convergence criteria for the geometry optimization were set to default values (OPT), and "tight" convergence criteria were used for SCF calculations (TIGHTSCF). The triple-ζ basis sets with one set of polarization functions[23] (TZVP) were used for transition-metal, O, and N atoms, and the double-ζ basis sets with one set of polarization functions[24] (SVP) were used for all other atoms. The resolution of the identity approximation (RIJCOSX) was employed[25,26] with matching

dx.doi.org/10.1021/ic4024713 | *Inorg. Chem.* 2014, 53, 1021−1031

auxiliary basis sets.[26] The conductor-like screening model (COSMO)[27] was used. All spin densities were calculated according to Löwdin population analysis.[28] Molecular orbitals and spin densities were visualized via the program *Molekel*.[29] Vibrational modes were analyzed by the program *gOpenMol*.[30]

X-ray Crystallography. Single crystals of [**1**]BF_4 were grown by layering of a dichloromethane solution with pentane at ambient temperatures, and those of [**2**]PF_6 were grown by the same method by storing the solution at −20 °C. Intensity data were collected at 100(2) K on a Bruker SMART AXS or a Bruker Kappa Apex II duo diffractometer (graphite-monochromated Mo Kα radiation, λ = 0.71073 Å). Crystallographic and experimental details for the structures are summarized in Table S1. Structures were solved by direct methods (*SHELXS-97*) and refined by full-matrix least-squares procedures (based on F^2, *SHELXL-97*).[31] CCDC 930441 and 930442 contain the CIF files for this manuscript. All data can be obtained free of charge from the Cambridge Crystallographic Data Centre via www.ccdc.cam.ac.uk/data_requests/cif.

■ ASSOCIATED CONTENT

Supporting Information

X-ray crystallographic data for complexes [**1**]BF_4 and [**2**]PF_6 in CIF format, EPR spectrum of $\mathbf{1}^{\bullet+}$ + PPh_3, solvent dependence of UV−vis−NIR spectra, calculated IR spectra, tables showing IR band assignments, and coordinates used for the DFT calculations. This material is available free of charge via the Internet at http://pubs.acs.org.

■ AUTHOR INFORMATION

Corresponding Authors

*E-mail: julia.weinstein@sheffield.ac.uk.

*E-mail: biprajit.sarkar@fu-berlin.de.

Notes

The authors declare no competing financial interest.

■ ACKNOWLEDGMENTS

We thank the EPSRC and the EPSRC E-Futures DTC (to M.D.), U.K., University of Sheffield, and STFC for support. The Carl-Zeiss Stiftung (doctoral stipend for N.D.) and Fonds der Chemischen Industrie (doctoral stipend for D.S.) are kindly acknowledged for financial support of this project.

■ REFERENCES

(1) (a) Cummings, S. D.; Eisenberg, R. *J. Am. Chem. Soc.* **1996**, *118*, 1949. (b) Zuleta, J. A.; Chesta, C. A.; Eisenberg, R. *J. Am. Chem. Soc.* **1989**, *111*, 8916. (c) Shavaleev, N. M.; Accorsi, G.; Virgili, D.; Bell, Z. R.; Lazarides, T.; Calogero, G.; Armaroli, N.; Ward, M. D. *Inorg. Chem.* **2005**, *44*, 61. (d) Volgler, A.; Kunkely, H. *J. Am. Chem. Soc.* **1981**, *103*, 1559. (e) Base, K.; Grinstaff, M. W. *Inorg. Chem.* **1998**, *37*, 1432. (f) Weinstein, J. A.; Zheligovskaya, N. N.; Mel'nikov, M. Y.; Hartl, F. *J. Chem. Soc., Dalton Trans.* **1998**, 2459.

(2) (a) Weinstein, J. A.; Tierney, M. T.; Davies, E. S.; Base, K.; Robeiro, A. A.; Grinstaff, M. W. *Inorg. Chem.* **2006**, *45*, 4544. (b) Shavaleev, N. M.; Davies, E. S.; Adams, H.; Best, J.; Weinstein, J. A. *Inorg. Chem.* **2008**, *47*, 1532. (c) Best, J.; Sazanovich, I. V.; Adams, H.; Bennett, R. D.; Davies, E. S.; Meijer, A. J. H. M.; Towrie, M.; Tikhomirov, S. A.; Bouganov, O. V.; Ward, M. D.; Weinstein, J. D. *Inorg. Chem.* **2010**, *49*, 10041. (d) Geary, E. A. M.; McCall, K. L.; Turner, A.; Murray, P. R.; McInnes, E. J. L.; Jack, L. A.; Yellowlees, L. J.; Robertson, N. *Dalton Trans.* **2008**, 3701. (e) Heinze, K.; Reinhardt, S. *Chem.—Eur. J.* **2008**, *14*, 9482. (f) Rauth, G. K.; Pal, S.; Das, D.; Sinha, C.; Slawin, A. M.; Woolins, J. D. *Polyhedron* **2001**, *20*, 363. (g) Sun, Z.; Chun, H.; Hildebrandt, K.; Boethe, E.; Weyhermüller, T.; Neese, F.; Wieghardt, K. *Inorg. Chem.* **2002**, *41*, 4295. (h) Ghosh, P.; Begum, A.; Herebian, D.; Boethe, E.; Hildebrand, K.; Weyhermüller, T.; Wieghardt, K. *Angew. Chem., Int. Ed.* **2003**, *42*, 563. (i) Mondal, S.; Paul, N.; Banerjee, P.; Mondal, T. K.; Goswami, S. *Dalton Trans.* **2010**, *39*, 2717.

(3) For selected examples, see: (a) Ward, M. D.; McCleverty, J. A. *J. Chem. Soc., Dalton Trans.* **2002**, 275. (b) Pierpont, C. G. *Coord. Chem. Rev.* **2001**, *216−217*, 95. (c) Zanello, P. *Coord. Chem. Rev.* **2006**, *50*, 2000. (d) Nomura, M.; Cauchy, T.; Fourmigué, M. *Coord. Chem. Rev.* **2010**, *254*, 1406. (e) Bonneval, B. G. d.; Ching, K. I. M. C.; Alary, F.; Bui, T.-T.; Valade, L. *Coord. Chem. Rev.* **2010**, *254*, 1457. (f) Chaudhuri, P.; Verani, C. N.; Bill, E.; Bothe, E.; Weyhermüller, T.; Wieghardt, K. *J. Am. Chem. Soc.* **2001**, *123*, 2213. (g) Bill, E.; Bothe, E.; Chaudhuri, P.; Chlopek, K.; Herebian, D.; Kokatam, S.; Ray, K.; Weyhermüller, T.; Neese, F.; Wieghardt, K. *Chem.—Eur. J.* **2005**, *11*, 204.

(4) For selected examples, see: (a) de Bruin, B.; Hetterscheid, D. G. H.; Koekkoek, A. J. J.; Grützmacher, H. *Prog. Inorg. Chem.* **2007**, *55*, 247. (b) Chirik, P. J.; Wieghardt, K. *Science* **2010**, *327*, 794. (c) Ringenberg, M. R.; Kokatam, S. L.; Heiden, Z. M.; Rauchfuss, T. B. *J. Am. Chem. Soc.* **2008**, *130*, 788. (d) Praneeth, V. K. K.; Ringenberg, M. R.; Ward, T. R. *Angew. Chem.* **2012**, *124*, 10374. (e) Dzik, W. I.; van der Vlugt, J. I.; Reek, J. N. H.; de Bruin, B. *Angew. Chem.* **2011**, *123*, 3416. (f) Nguyen, A. I.; Blackmore, K. J.; Carter, S. M.; Zarkesh, R. A.; Heyduk, A. F. *J. Am. Chem. Soc.* **2009**, *131*, 3307. (g) Tsai, M. K.; Rochford, J.; Polyansky, D. E.; Wada, T.; Tanaka, K.; Muckerman, J. T. *Inorg. Chem.* **2009**, *48*, 4372. (h) Forum Issue on Redox-Active Ligands: *Inorg. Chem.* **2011**, *50*, 9737−9914. (i) *Eur. J. Inorg. Chem.* **2012**, 340−580. (j) Luca, O. R.; Crabtree, R. H. *Chem. Soc. Rev.* **2013**, *42*, 1440. (k) Boyer, J. L.; Cundari, T. R.; DeYonker, N. J.; Rauchfuss, T. B.; Wilson, S. R. *Inorg. Chem.* **2009**, *48*, 638. (l) Tondreau, A. M.; Atienza, C. C. H.; Weller, K. J.; Nye, S. A.; Lewis, K. M.; Delis, J. G. P.; Chirik, P. J. *Science* **2012**, *335*, 567.

(5) Samanta, S.; Ghosh, P.; Goswami, S. *Dalton Trans.* **2012**, *41*, 2213.

(6) Poddel'sky, A. I.; Cherkasov, V. K.; Abakumov, G. A. *Coord. Chem. Rev.* **2009**, *253*, 291.

(7) (a) Roy, S.; Hartenbach, I.; Sarkar, B. *Eur. J. Inorg. Chem.* **2009**, 2553. (b) Sarkar, B.; Huebner, R.; Pattacini, R.; Hartenbach, I. *Dalton Trans.* **2009**, 4653. (c) Deibel, N.; Schweinfurth, D.; Fiedler, J.; Zalis, S.; Sarkar, B. *Dalton Trans.* **2011**, *40*, 9925. (d) Deibel, N.; Schweinfurth, D.; Hohloch, S.; Fiedler, J.; Sarkar, B. *Chem. Commun.* **2012**, *48*, 2388.

(8) Bhattacharya, S.; Gupta, P.; Basuli, F.; Pierpont, C. G. *Inorg. Chem.* **2002**, *41*, 5810.

(9) Brown, S. N. *Inorg. Chem.* **2012**, *51*, 1251.

(10) Abakumov, G. A.; Teplova, I. A.; Cherkasov, V. K.; Shalnova, K. G. *Inorg. Chim. Acta* **1979**, *32*, L57.

(11) (a) Lever, A. B. P. *Inorganic electronic spectroscopy*, 2nd ed.; Elsevier: Amsterdam, The Netherlands, 1984. (b) Manuta, D. M.; Lees, A. J. *Inorg. Chem.* **1986**, *25*, 3212.

(12) Weil, J. A.; Bolton, J. R.; Wertz, J. E. *Electron Paramagnetic Resonance*; Wiley: New York, 1994.

(13) Archer, S.; Weinstein, J. A. *Coord. Chem. Rev.* **2012**, *256*, 2530.

(14) Taylor, A. J.; Davies, E. S.; Weinstein, J. A.; Sazanovich, I. V.; Bouganov, O. V.; Tikhomirov, S. A.; Towrie, M.; McMaster, J.; Garner, C. D. *Inorg. Chem.* **2012**, *51*, 13181.

(15) Adams, C. J.; Fey, N.; Harrison, Z. A.; Sazanovich, I. V; Towrie, M.; Weinstein, J. A. *Inorg. Chem.* **2008**, *47*, 8242.

(16) Sazanovich, I. V.; Alamiry, M. A. H.; Best, J.; Bennett, R. D.; Bouganov, O. V.; Davies, E. S.; Grivin, V. P.; Meijer, A. J. H. M.; Plyusnin, V. F.; Ronayne, K. L.; Shelton, A. H.; Tikhomirov, S. A.; Towrie, M.; Weinstein, J. A. *Inorg. Chem.* **2008**, *47*, 10432.

(17) (a) Glik, E. A.; Kinayyigit, S.; Ronayne, K. L.; Towrie, M.; Sazanovich, I. V.; Weinstein, J. A.; Castellano, F. N. *Inorg. Chem.* **2008**, *47*, 6974. (b) Weinstein, J. A.; Grills, D. C.; Towrie, M.; Matousek, P.; Parker, A. W.; George, M. W. *J. Chem. Soc., Chem. Commun.* **2002**, 382.

(18) Krejcik, M.; Danek, M.; Hartl, F. *J. Electroanal. Chem.* **1991**, *317*, 179.

(19) Greetham, G.; Burgos, P.; Cao, Q.; Clark, I.; Codd, P.; Farrow, R.; George, M.; Kogimtzis, M.; Matousek, P.; Parker, A.; Pollard, M.; Robinson, D.; Xin, Z.-J.; Towrie, M. *Appl. Spectrosc.* **2010**, *64*, 1311.

(20) Neese, F. *ORCA: An Ab Initio, Density Functional and Semiempirical Program Package*, version 2.9.1; Department of Molecular Theory and Spectroscopy, Max Planck Institute for Bioinorganic Chemistry: Mülheim/Ruhr, Germany, Jan 2012.
(21) (a) Becke, A. D. *J. Chem. Phys.* **1993**, *98*, 5648. (b) Lee, C. T.; Yang, W. T.; Parr, R. G. *Phys. Rev. B* **1988**, *37*, 785.
(22) van Wüllen, C. *J. Chem. Phys.* **1998**, *109*, 392.
(23) Schafer, A.; Huber, C.; Ahlrichs, R. *J. Chem. Phys.* **1994**, *100*, 5829.
(24) Schafer, A.; Horn, H.; Ahlrichs, R. *J. Chem. Phys.* **1992**, *97*, 2571.
(25) (a) Baerends, E. J.; Ellis, D. E.; Ros, P. *Chem. Phys.* **1973**, *2*, 41. (b) Dunlap, B. I.; Connolly, J. W. D.; Sabin, J. R. *J. Chem. Phys.* **1979**, *71*, 3396. (c) Vahtras, O.; Almlof, J.; Feyereisen, M. W. *Chem. Phys. Lett.* **1993**, *213*, 514.
(26) (a) Eichkorn, K.; Greutler, O. T.; Ohm, H.; Haser, M.; Ahlrichs, R. *Chem. Phys. Lett.* **1995**, *242*, 652. (b) Eichkorn, K.; Weigend, F.; Treutler, O.; Ahlrichs, R. *Theor. Chem. Acc.* **1997**, *97*, 119.
(27) Klamt, A.; Schüürmann, G. *J. Chem. Soc., Perkin Trans. 2* **1993**, 799.
(28) (a) Löwdin, P. O. *J. Chem. Phys.* **1950**, *18*, 365. (b) Löwdin, P. O. *Adv. Quantum Chem.* **1970**, *5*, 185.
(29) Portmann, S. *Molekel*, version 5.4.0.8; CSCS/UNI Geneva: Geneva, Switzerland, 2009.
(30) (a) Laaksonen, L. *J. Mol. Graph.* **1992**, *10*, 33. (b) Bermann, D. L.; Laaksonen, A. *J. Mol. Graph. Model* **1997**, *15*, 301.
(31) Sheldrick, G. M. *SHELXL-97, Program for refinement of crystal structures*; University of Göttingen, Göttingen, Germany, 1997.

dx.doi.org/10.1021/ic4024713 | *Inorg. Chem.* 2014, 53, 1021−1031